AD-A070 358 NORTH CAROLINA STATE UNIV RALEIGH DEPT OF ELECTRICAL--ETC F/G 4/1
D REGION AMPLITUDE DISTRIBUTION, CONE ANGLE OF ARRIVAL, AND ELE--ETC(U)
JUN 79 W A FLOOD, H N TURNER, T F SHIRLEY DAHC04-74-G-0161
UNCLASSIFIED ARO-11054.1-GS NL

| OF |
AD
A070358

END
DATE
FILMED
7-79
DDC

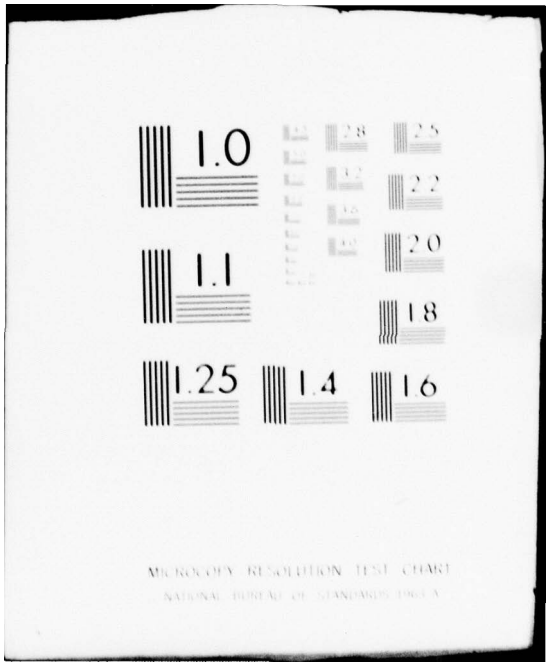
1.0
1.1
1.25
1.4
1.6
2.8
2.5
2.2
2.0
1.8
MICROCOPY RESOLUTION TEST CHART
NATIONAL BUREAU OF STANDARDS 1963-A

ARO. 11054.1-GS

(12)

"D Region Amplitude Distributions, Cone Angle of Arrival, and Electron Density Profiles"

Final Report

W. A. Flood
H. N. Turner
T. F. Shirley

June 1979

U. S. Army Research Office

Grants: DAHCO4 74 G 0161

and

DAAG29 76 G 0138

Department of Electrical Engineering
North Carolina State University
Raleigh, N. C.

SECURITY CLASSIFICATION OF THIS PAGE (When Data Entered)

REPORT DOCUMENTATION PAGE

READ INSTRUCTIONS BEFORE COMPLETING FORM

1. REPORT NUMBER: 11054-EN
2. GOVT ACCESSION NO.:
3. RECIPIENT'S CATALOG NUMBER:

4. TITLE (and Subtitle): D Region Amplitude Distribution, Cone Angle of Arrival, and Electron Density Profiles.

5. TYPE OF REPORT & PERIOD COVERED: Final Report. 1974-1978.

6. PERFORMING ORG. REPORT NUMBER: —

7. AUTHOR(s): W. A. Flood, H. N. Turner, T. F. Shirley

8. CONTRACT OR GRANT NUMBER(s): DAHC04-74-G0161, DAAG29-76-G0138

9. PERFORMING ORGANIZATION NAME AND ADDRESS:
Department of Electrical Engineering
N. C. State University
Raleigh, NC 27650

10. PROGRAM ELEMENT, PROJECT, TASK AREA & WORK UNIT NUMBERS: 11054-EN

11. CONTROLLING OFFICE NAME AND ADDRESS:
U. S. Army Research Office
Post Office Box 12211
Research Triangle Park, NC 27709

12. REPORT DATE: June 1979

13. NUMBER OF PAGES: 47p.

14. MONITORING AGENCY NAME & ADDRESS (if different from Controlling Office)

15. SECURITY CLASS. (of this report): Unclassified

15a. DECLASSIFICATION/DOWNGRADING SCHEDULE: NA

16. DISTRIBUTION STATEMENT (of this Report)

Approved for public release; distribution unlimited.

17. DISTRIBUTION STATEMENT (of the abstract entered in Block 20, if different from Report)

NA

18. ARO

19. 11054.1-GS

18. SUPPLEMENTARY NOTES

The findings in this report are not to be construed as an official Department of the Army position, unless so designated by other authorized documents.

19. KEY WORDS (Continue on reverse side if necessary and identify by block number)

D Region Backscatter, Partial Reflection Experiment,
D Region Electron Density Profiles.

404 862

20. ABSTRACT (Continue on reverse side if necessary and identify by block number)

The results of analytical and experimental investigations of D region backscattering processes and their effects on the accuracy of electron density profiles produced by the partial reflection technique are presented. The major findings were that the cone angle of arrival of D region echoes is approximately 13 degrees but on occasion can be significantly greater for both O and X polarizations; in the altitude regime between 74 and 80 kilometers, X-wave

DD FORM 1 JAN 73 1473 * EDITION OF 1 NOV 65 IS OBSOLETE

cone angles can be greater than 0 wave cone angles of arrival and this phenomenon is associated with local minima in the electron density profiles; the cone angle of arrival can be large enough that altitude resolution of the experiment is determined by the D region backscatter and not by the pulse length of the transmitter. D region echoes were shown to be Rayleigh distributed lending support to the concept of volume scattering from fluctuations of refractive index. Finally the seasonal variation of D region electron density profiles was established.

Table of Contents

List of Tables

List of Figures

Introduction

The goals of this research program were to determine the characteristics of D region (60-90 kilometers) backscattering and the effects of these characteristics upon the accuracy of experimentally derived D region electron density profiles and D region "winds." Five particular goals were:

(1) The investigation of the validity of the randomly phased angular spectrum approximation (here-after abbreviated RPASA).
(2) The measurement of the cone angle of arrival of D region echoes.
(3) The effects of the cone angle of arrival echoes the accuracy of D region electron density profiles and "winds."
(4) Measurement of the amplitude distribution of D region echoes.
(5) Measurement of D region electron density profiles to establish seasonal variations.

1. The Validity of the RPASA

The electric field intensity, measured on the ground, of waves backscattered from the ionosphere can be described by a spectrum (in angle space) of plane waves. The Fourier transform of this angular spectrum is the spatial correlation function of the electric-field intensity measured in the observation plane. The normalized correlation function is defined by a spatial average:

$$p(\Delta x,\Delta y) = \lim_{\substack{L_x \to \infty \\ L_y \to \infty}} \frac{\frac{1}{4L_xL_y}\int_{-L_x}^{L_x}\int_{-L_y}^{L_y} E(x,y,z)E^*(x+\Delta y,z)\,dydx}{\frac{1}{4L_xL_y}\int_{-L_x}^{L_x}\int_{-L_y}^{L_y} |E(x,y,z)|^2 dydx} \qquad (1.1)$$

The infinite spatial average required to evaluate (1.1) is impossible to perform in a real world. Yet, the spatial correlation function plays a critical role in measuring "winds" by means of the ionospheric drift technique. In the ionospheric drift technique, measurements from at least three receivers are used to deduce the spatial correlation function from a temporal average:

$$R(\Delta x,\Delta y) = \lim_{T \to \infty} \frac{\frac{1}{T}\int_{-T/2}^{T/2} E(x,y,z,t)E^*(x+\Delta x_3 y+\Delta y,z,t)\,dt}{\frac{1}{T}\int_{-T/2}^{T/2} |E(x,y,z,t)|^2_{\phi\tau}} \qquad (1.2)$$

It should be clear that equation (1.2) has an explicit dependence on the absolute dependence (x,y,z) as Δx and Δy. Nonetheless, experimenters equate equations (1.1) and (1.2). One can show that the only way this can be true is if the angular spectrum is randomly phased -- that is if:

$$\overline{F(s_1,s_2,t)\ F^{*}(s_1',s_2',t)} = \overline{|F(s_1,s_2,t)|^2}\ \delta(s_1-s_1')\ \delta(s_2-s_2') \qquad (1.3)$$

where $F(s_1,s_2,t)$ is a component of the angular spectrum of plane waves having complex amplitude $F(s_1,s_2,t)$ traveling in a direction specified by direction cosines s_1,s_2,s_3 where:

$$s_1^2 + s_2^2 + s_3^2 = 1 \qquad (1.4)$$

One can also show that no physically realizable angular spectrum can be exactly randomly phased, but that a spectrum may be approximately randomly phased so that equating (1.2) and (1.1) may be justified for relatively small values of Δx and Δy.

There has been only one experimental investigation of the validity of the RPASA. Von Biel (1969) developed a technique to measure the spatial correlation of the complex fields reflected from the ionosphere. Using nearly normal incidence echoes in New Zealand, von Biel concluded that D region echoes did <u>not</u> have a randomly phased angular spectrum.

We implemented von Biel's technique at Raleigh, NC with a 100 kw (peak pulse power) 2.66 MHz transmitter, a circularly polarized transmitting array and five half wave dipoles separated by $\lambda/2$ spacing. A necessary condition for the validity of the RPSASA is that measured correlation functions (say for a spacing of a half wavelength) should be independent of position. Our

array of 5 dipoles spaced a half wavelength apart permitted a determination of four measurements of the complex correlation coefficient evaluated for one half wave length separation over a range of absolute positions which extended to 2 wavelengths.

Variations in the four correlation measurements can be caused by sampling errors, noise and interference, or a true position dependence. An analysis was performed (by HNT) which showed that unless the signal to interference ratio was very high, the phase of the measured correlation function was subject to serious error. Furthermore, at large separation distances, where the magnitude of the correlation function is small, relatively low levels of interference can cause large errors in the measurement of the magnitude of the correlation function. However, for signal to interference ratios of greater than 10 db and for separations such that the magnitude of the true correlation is not small, the effect of interference on the measured magnitude of the correlation function is tolerable.

Using records taken on days of exceptionally low interference levels, reduction of the averaging time from 20 to 5 minutes produced changes of less than 3% in magnitude of the correlation function. Variations of approximately 3% are charged to sampling error. Data processing was restricted to records of 20 minute duration at altitudes where the signal to interference ratio was greater than 10 db. Some measurements of the phase as well as the magnitude of the correlation

function were obtained on days of exceptionally low noise and examples will be shown.

Data acquired during the period May, 1976, through October, 1976, consisted of 20 minute data runs taken around local noon. Pulse repetition frequencies of 16 pulses per second were used and measurements were made at two kilometer intervals in the altitude range 60-100 kilometers.

A measure of the variability of the four values of correlation magnitudes for each run is the percent standard deviation (PSD).

$$PSD = \frac{\sigma}{M} \times 100\% \qquad (1.4)$$

where M and σ are the mean and standard deviation for that data run.

A summary of the correlation data as a function of altitude is presented in Table 1.1. N is the number of individual 20 minute observations used at each altitude, and $\bar{M}$ and $\overline{PSD}$ are the averages of the N means and the N standard deviations at each altitude. The largest PSD value and its associated mean is also listed for each altitude. The largest values of PSD for six of the sixteen altitudes were the result of a single 20 minute observation. The low values of the average PSD ($\overline{PSD}$) indicate that the remaining PSD's were much lower (at least for those altitudes with more than one observation). We conclude that at all altitudes, the magnitude of the complex correlatlion function for spatial

Table 1.1 Summary of Position Dependence Data

h	N	M	PSD	Maximum PSD	Related M
68	5	0.787	3.41%	5.9 %	0.839
70	5	0.795	4.98%	14.9 %	0.686
72	5	0.700	4.94%	13.3 %	0.660
74	4	0.692	5.68%	11.4 %	0.700
76	1	0.621	8.29%	8.29%	0.621
78	1	0.529	28.90%	28.90%	0.529
80	1	0.829	1.91%	1.91%	0.829
82	3	0.803	4.13%	6.27%	0.683
84	6	0.820	2.49%	4.70%	0.788
86	7	0.855	2.23%	3.27%	0.845
88	10	0.834	3.14%	6.97%	0.797
90	16	0.826	2.77%	6.46%	0.888
92	18	0.809	3.85%	10.0 %	0.710
94	18	0.784	4.71%	6.17%	0.713
96	15	0.776	3.53%	6.42%	0.727
98	14	0.757	4.70%	8.28%	0.628

separations of $\lambda/2$ is essentially independent of position at least over the 2λ range of absolute positions used in this experiment.

To the extent that the magnitude of the correlation function is independent of position, the RPASA is valid. However, the phase of the correlation function has not been shown to be independent of position, since, except on rare occasions, the signal to interference ratio of D region echoes was not large enough to permit reliable phase measurements. An example of such a rare occasion is shown in Figure 1.1.

In Figure 1.1, the magnitudes of the correlation functions for each pair of observing stations at each altitude are closely grouped as might be expected for a complex correlation function which is independent of position. The phase plots have the same form, but there are obvious offsets between them. (The similarity of the phase plots is indicative of the fact that interference levels were well below D region echo levels.)

1.1 E Region Tests of System Operation. Echoes from a quiet E region, characterized by steady or very slowly fading amplitudes from a very restricted range of altitudes, were used to test system operation. Figure 1.2 is a plot of the magnitude and phase of the complex correlation function of an echo from the quiet E region. The correlation function was evaluated for spacings of $\lambda/2$, λ, $\frac{3\lambda}{2}$, and 2λ and the individual data points have been connected by straight lines.

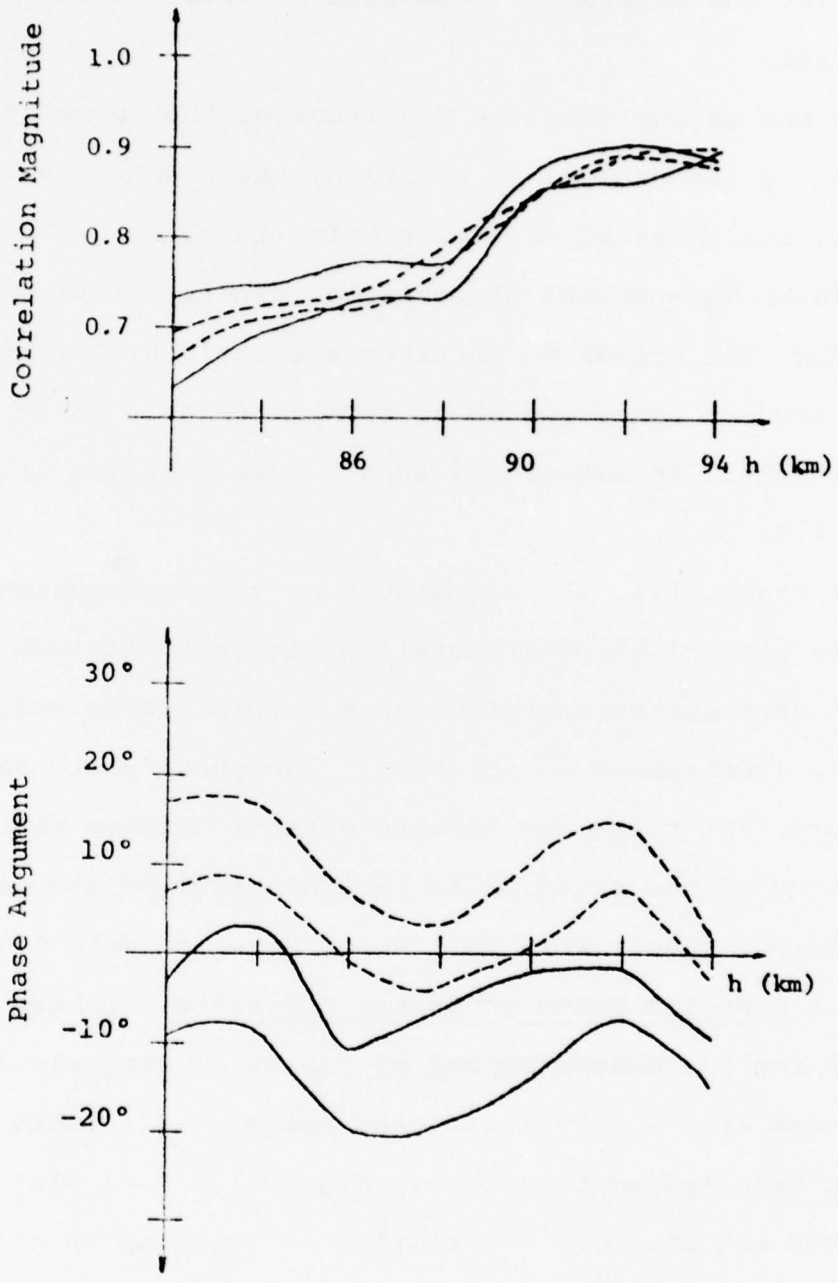

Figure 1.1 Correlation magnitudes and phases vs. altitude at four positions of λ/2 separation.

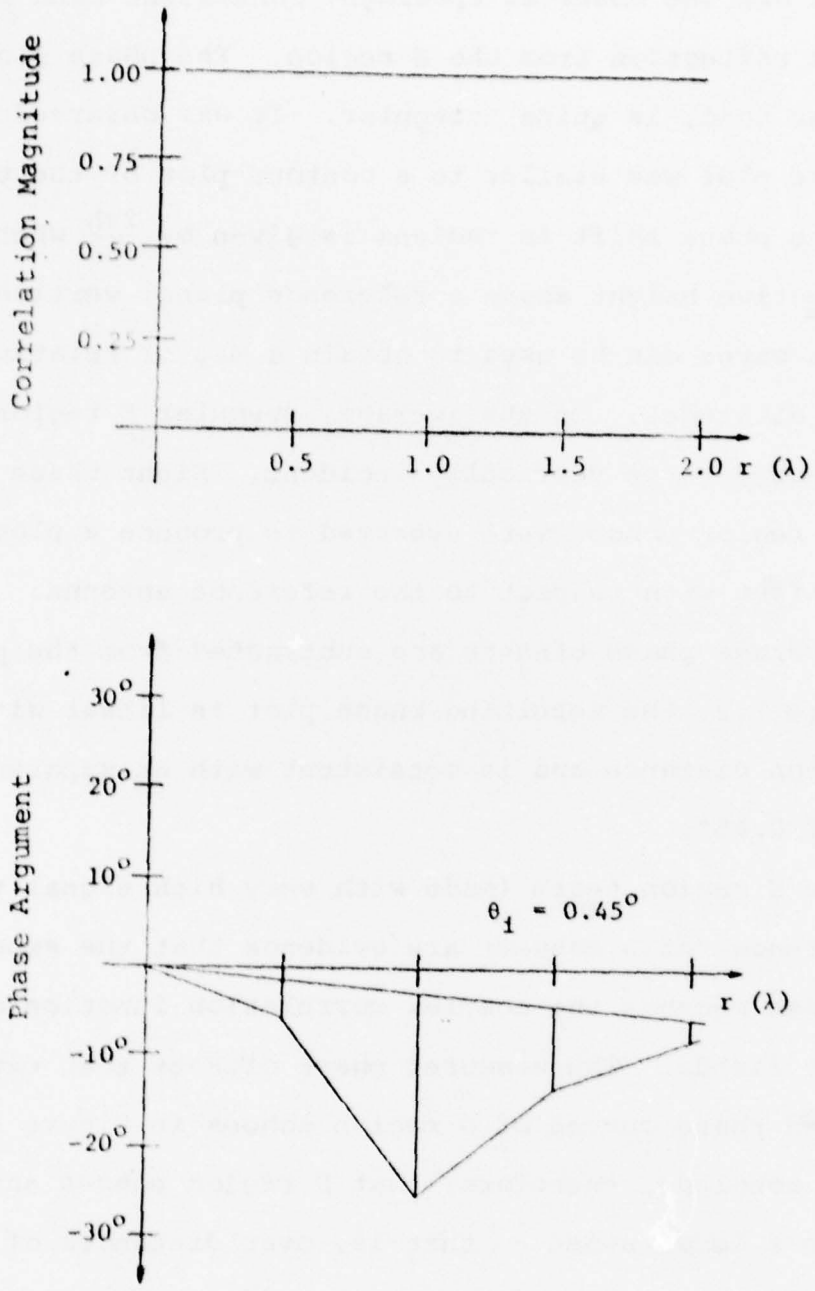

Figure 1.2 E-region spatial correlation function.

The magnitude of the correlation function is essentially unity at all the observed spacings, consistent with a nearly specular reflection from the E region. The phase plot, on the other hand, is quite irregular. It was observed that the phase plot was similar to a contour plot of the test site. Since the phase shift in radians is given by $\frac{2\pi h}{\lambda}$ where h is the effective height above a reference plane, vertically incident waves can be used to obtain a map of relative antenna altitudes. On the average, specular E region returns are expected to be vertically incident. Eight phase plots of quiet E region echoes were averaged to produce a plot of average phase offset with respect to the reference antenna. When these average phase offsets are subtracted from the phases plotted in Figure 1.2, the resulting phase plot is linear with separation distance and is consistent with an apparent zenith angle of 0.45°.

The E region tests (made with very high signal to interference ratio echoes) are evidence that the experimental system can measure the complex correlation function of the incident fields. The measured phase offsets then explain the displaced phase curves of D region echoes in Figure 1.1.

We conclude, therefore, that D region echoes satisfy the RPASA in a local sense -- that is, over distances of at least two wavelenghts, the RPASA seems valid. Equating equations (1.1) and (1.2) seems valid -- at least for the Raleigh area.

2. Cone Angle of Arrival of D Region Echoes

The array of five dipole antennas and the validity of the RPASA make possible the estimation of the half power width of the angular power spectrum. The angular spectrum is denoted by:

$\overline{|F(s_1,s_2,t))|^2}ds_1ds_2$ = power density associated with a plane wave with direction cosines s_1, s_2, and s_3.

The angular power spectrum and the spatial correlation function, (1.1), are Fourier transform pairs. Assume that the two dimensional correlation function is isotropic and is of the form:

$$p(\Delta x,\Delta y) = \exp\{-B^2[(\Delta x)^2 + (\Delta y^2)]\} = \exp\{-B^2r^2\} \qquad (2.1)$$

where $r^2 = (\Delta x)^2 + (\Delta y)^2$

The one dimensional (isotropic) angular power spectrum is:

$$\overline{|F(s)|^2} = \frac{\pi}{B^2}\exp\{-(\frac{\pi s}{B})^2\} \qquad (2.2)$$

where $\overline{|F(s)|^2}$ is the angular power spectrum of the backscattered echoes as a function of s, the sine of the zenith angle. We define the half power width of the angular spectrum by:

$$\frac{\overline{|F(s_{1/2})|^2}}{\overline{|F(0)|^2}} = 0.5 \qquad (2.3)$$

where $s_{1/2} = \sin\theta_{1/2} = \frac{B}{\pi}\sqrt{\ell n 2} = .27B \qquad (2.4)$

Least squared fits of the experimentally determined spatial correlation function for separations of 1/2, 1, and 1 1/2, wavelengths were made to estimate the parameter B^2 in equation (2.1) and these estimates used to determine the half power angle of D region echoes from equation (2.4).

In Section 1, an analysis of the effects of interference on the determination of the magnitude and phase of the spatial correlation function was used to show that even when signal to interference ratios were high, the magnitude of the spatial correlation function evaluated at large separations (where the magnitude value is low) is likely to be in error due to interference. Almost all values of the magnitude of D region spatial correlation functions at the two wavelength separations were too low to use in the least squared fitting procedure.

Figure 2.1 is a plot of the magnitude of the spatial correlation function at altitudes of 68, 72, and 76 kilometers. It is not an a-typical set of curves. The rms error in fitting the data points for the 72 km curve at $\lambda/2$, λ, and $3\lambda/2$ was .0234. The possible rms error caused by interference was estimated to be .058. Since the error in the curve fit is less than might be expected due to interference, (2.1) is said to be a "good" fit to the 72 kilometer correlation data and the cone estimate is likewise classified "good." Because similar error values were found for many other spatial correlation curves, it was concluded that (2.1) is adequate for cone angle estimation provided that the signal to inter-

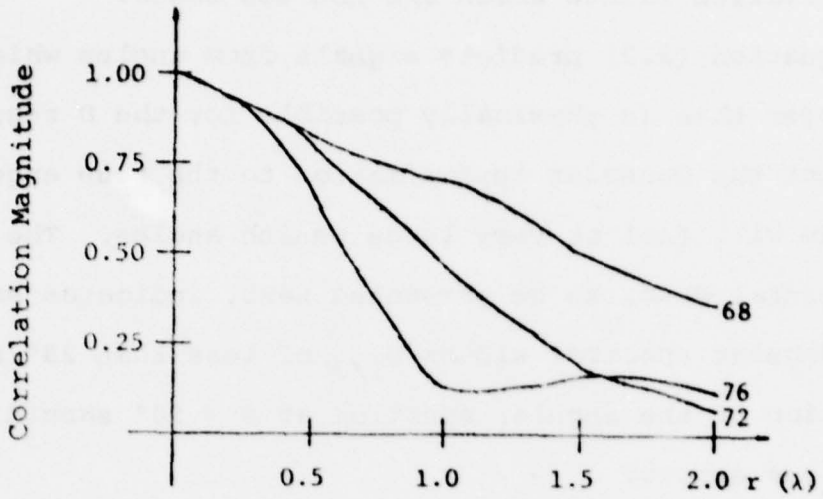

Figure 2.1 D-region spatial correlation function.

ference ratio is greater than 10 db and the fit is limited to correlation values which are not too small.

Equation (2.2) predicts signals from angles which are larger than is physically possible for the D region. We expect the Gaussian approximation to the true angular spectrum will fail at very large zenith angles. The experimental data, to be presented next, indicates half power angular spectral widths, $\theta_{1/2}$, of less than 25° so that truncation of the angular spectrum at $\theta = 90°$ should cause no serious errors.

2.1 Summary of Cone Angle Results. The cone angle data obtained from D region measurements made around local noon during the period May 1976, through October 1976, are plotted in Figure 2.2. For each altitude, Table 2.1 lists the following:

N = number of cone angle estimates at each altitude

$\bar{\theta}_{1/2}$ = mean of the N estimates at each altitude

$\sigma_{1/2}$ = standard deviation of the N estimates

$\theta_{1/2\,max}$ = largest of the N estimates of the half power width at that altitude

The most striking feature of Figure 2.2 and Table 2.1 is the rapid rise in cone angle between 68 and 78 kilometers. Most of the data below 78 kilometers were obtained with x wave polarization because of the generally stronger x wave returns at lower altitudes. The increase in cone angles between 68 and 78 kilometers is probably caused by the rapid rise in X-wave absorption which causes the X wave amplitude

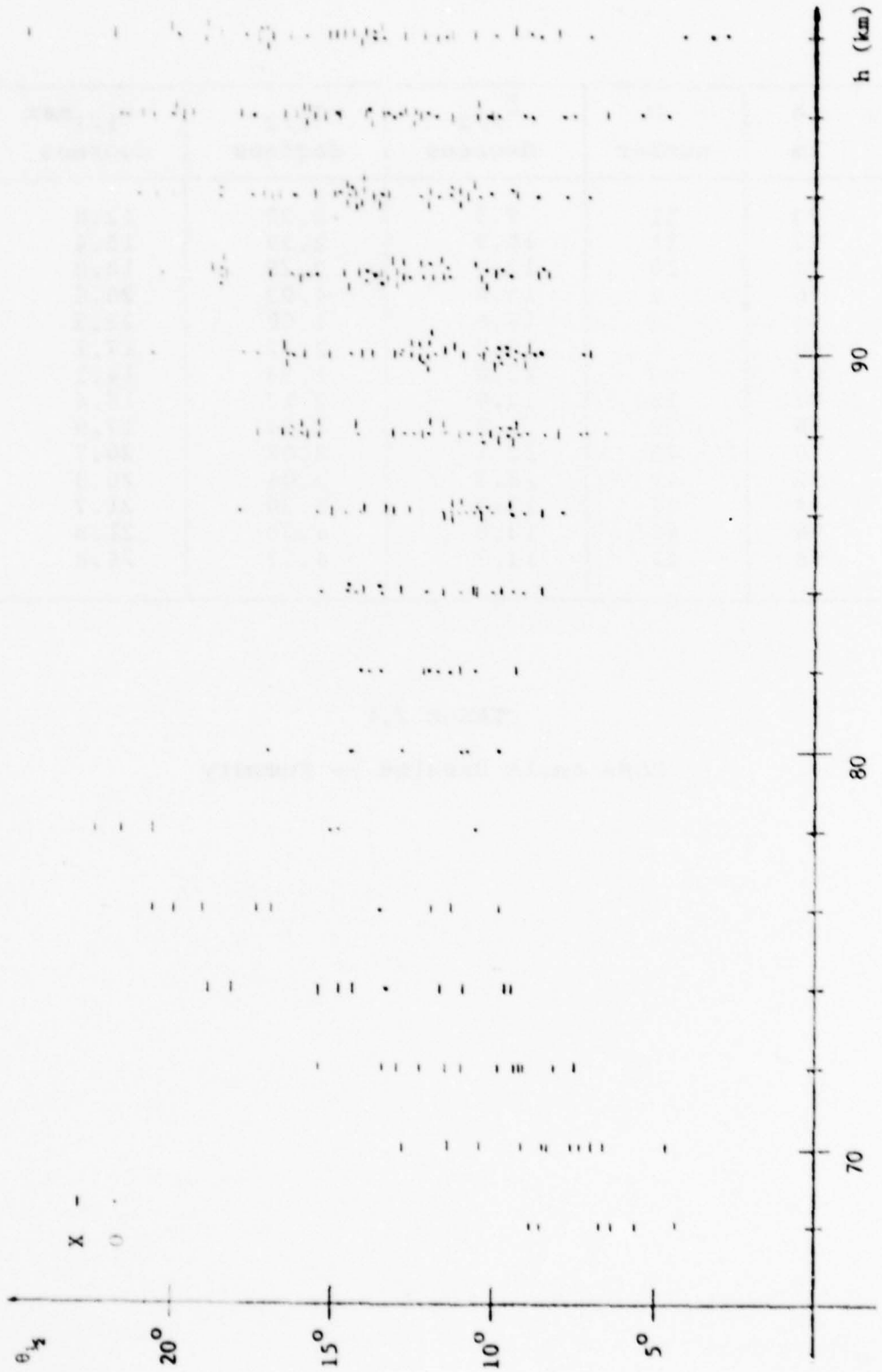

Figure 2.2 Cone angle summary.

h km	N number	$\bar{\theta}_{1/2}$ degrees	$\sigma_{1/2}$ degrees	$\theta_{1/2}^{max}$ degrees
70	11	8.5	2.32	12.8
72	11	10.9	2.39	15.4
74	10	13.7	3.28	18.8
76	9	15.6	4.02	20.6
78	6	17,6	4.68	22.3
80	6	12.7	2.72	17.1
82	10	12.0	1.53	14.1
84	18	12.0	2.17	15.4
86	30	11.8	2.24	17.9
90	45	12.1	3.08	20.7
92	49	13.3	3.04	20.3
94	47	13.7	3.30	21.7
96	48	13.8	4.30	21.8
98	41	13.7	4.77	24.8

TABLE 2.1

Cone Angle Results -- Summary

to decrease with increasing altitude. Consequently, stronger x wave echoes at lower altitudes (and larger zenith angles) tend to dominate the measurement so that over the range 68-78 kilometers, the cone angle of arrival increases.

Above 82 kilometers, where both the X and O wave amplitudes increase with altitude, the mean cone angle is approximately constant at 12-13 degrees. The standard deviation, $\sigma_{1/2}$, increases with altitude. Note that the higher altitude data have very high signal to interference ratios so that interference can be eliminated as the cause of the increased cone angle variability at the higher altitudes.

3. Effects of Cone Angle Results on the Partial Reflection Experiment

3.1 Altitude Smearing and Pulse Length. D-region echoes are frequently assumed to come from a horizontal slab of thickness L($L = \frac{c\tau}{2}$ where c is the vacuum velocity of light and τ is the pulse duration) centered at a height R_o. Because of the curvature of the wave front, not all of the scattering volume is contained within the slab. The percentage of the scattering volume contained in the horizontal slab is most important in assessing altitude "smearing."

Cross sections of two scattering volumes are shown in Figure 3.1. The volumes are portions of spherical shells of thickness L. The angular width of the shells is $\theta_{1/2}$, and the figure illustrates the cases $\theta_{1/2} < \theta_B$ and

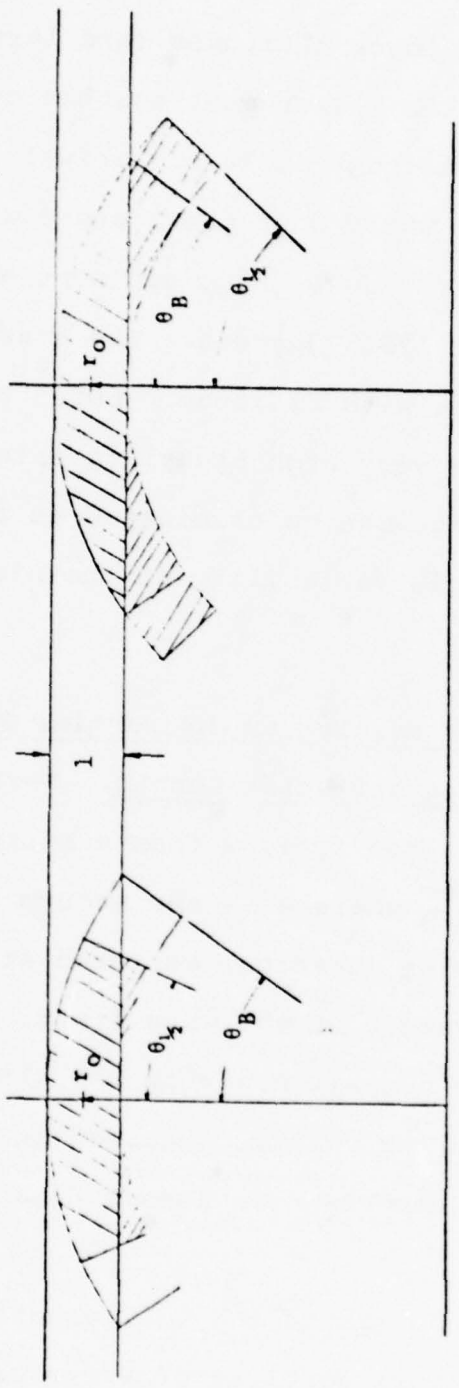

Figure 3.1 Scattering volume diagrams.

$\theta_{1/2} > \theta_B$ where θ_B is the angle at which the outer edge of the spherical shell is at the height of the bottom of the horizontal slab.

$$\theta_B = \cos^{-1}\left\{\frac{R_o - L/2}{R_o + L/2}\right\} \tag{3.1}$$

The total volume of the shell section is:

$$V_{tot} = \frac{2\pi}{3}(1-\cos\theta_{1/2})(3R_o^2L + \frac{L^3}{4}) \tag{3.2}$$

The volume of the shell section inside the horizontal slab is V_s:

$$V_s = \frac{2\pi}{3}(1-\cos\theta_{1/2})(R_o+L/2)^3 - 1/2\ \tan^2\theta_{1/2}(R_o-L/2)^3] \text{ for } \theta_{1/2} < \theta_B$$

$$V_s = \frac{2\pi}{3}(1-\cos\theta_B)(R_o+L/2)^3 - 1/2\ \tan^2\theta_{1/2}(R_o-L/2)^3 \text{ for } \theta_{1/2} > \theta_B \tag{3.3}$$

The percent volume in the horizontal slab is

$$V_s\% = \frac{V_s}{V_{tot}} \times 100\% \tag{3.4}$$

Values of $V_s\%$ are listed in Table 3.1(a) for several values of pulse length and angle $\theta_{1/2}$. Of interest are the angles $\theta_{1/2}$ where fifty percent of the scattering volume is inside the horizontal slab such that

$$V_s\% = 50\%.$$

Table 3.1(b) lists examples of $\theta_{1/2}$ which satisfy (3.5) for several heights and pulse lengths. The angles θ_B are also listed for each height. It can be seen that the angle which satisfies the condition (3.5) is given approximately by θ_B for 2 to 4 km pulse lengths.

TABLE 3.1.a

Scattering Volume Percentages

	V_s% for L = 4 km				V_s% for L = 2 km			
r_o	θ_B	$\theta_{\frac{1}{2}}=9^o$	$\theta_{\frac{1}{2}}=13^o$	$\theta_{\frac{1}{2}}=17^o$	θ_B	$\theta_{\frac{1}{2}}=9^o$	$\theta_{\frac{1}{2}}=13^o$	$\theta_{\frac{1}{2}}=17^o$
68	19.5°	90.3%	79.4%	64.0%	13.8°	79.6%	56.9%	33.8%
74	18.7°	89.3%	77.4%	60.5%	13.3°	77.8%	52.9%	31.1%
80	18.0°	88.4%	75.4%	57.0%	12.8°	75.9%	49.0%	28.7%
86	17.3°	87.5%	73.4%	53.5%	12.3°	74.0%	45.5%	26.7%

TABLE 3.1.b

r_o	L	θ_B	50% $\theta_{1/2}$
68	4	19.5°	19.8°
86	4	17.3°	17.6°
68	2	13.8°	14.0°

As the cone angle $\theta_{1/2}$ approaches θ_B, approximately 50% of the scattering volume lies at altitudes below the horizontal slab and significant altitude smearing is present (in excess of that expected from the spatial extent $\frac{c\tau}{2}$). The cone angle data of the previous section suggest that for X waves, increased altitude smearing is present at ranges where $\bar{A}_x$ decreases with altitude. Consequently, regions where $\frac{\partial \bar{A}_x}{\partial R}$ is negative can present problems for the partial reflection experiment.

One property of the scattering volume apparent from Table 3.1 is that for a given cone angle $\theta_{1/2}$, shorter pulse lengths have a smaller percentage of the total volume in the correct horizontal slab. While the actual altitude resolution is improved by using shorter pulse lengths, the relative effect of a given cone angle is greater for shorter pulses.

3.2 The Effect of Oblique Echoes on the $\bar{A}_x/\bar{A}_o$ Ratio. In view of the potential seriousness of differing cone angles for O and X polarizations, some estimate of the effect of this difference on the partial reflection experiment is necessary. Table 3.2 presents results of a cone angle data run for X-wave polarization where $\overline{|E_x|^2}$ is the mean of the square of the amplitude as a function of altitude from 68-76 km. Also shown in the table are measured values of the cone angle $\theta_{1/2}$ and calculated values of θ_B and $V_s\%(\theta_{1/2})$.

Table 3.2 Relative Power as a Function of Altitude

R_o	$\overline{\lvert E_x \rvert^2}$	$\theta_{1/2}$	θ_B	$V_s\%$ $(\theta_{1/2})$
68	2326	8.5°	19.5°	91.3%
70	3987	10.4°	19.2°	86.5%
72	4103	13.2°	18.9°	77.4%
74	3141	17.8°	18.7°	56.5%
76	2295	20.5°	18.4°	41.9%

First note that the mean squared wave amplitude increases from 68-72 km and then decreases from 72 to 76 km. The cone angles appear to increase with increasing altitude and exceed 13 degrees, the mean cone angle associated with the O wave (see Section 2) at altitudes above 72 km. At altitudes of 76 km and above the cone angle is greater than θ_B. Cone angle estimates for O-wave echoes below 80 km could not be made because of low signal amplitudes for this polarization, but it is assumed that such estimates would be less than the 13 degree mean O-wave cone angle.

The situation is as follows: X waves are scattered from a spherical shell with a cone angle varying from 13° to 20.5° as the altitude increases from 72 to 76 km, whereas the O waves are coming from a spherical shell with a cone angle of 13 degrees at all altitudes. The scattering volumes for the X and O waves are different. The problem is further complicated by the fact that the scattering cross-section per unit volume for each polarization is also a function of altitude.

The ratio of the power backscattered by the O and X modes is proportional to the ratio of the scattering volumes for both modes. We ask by what factor must the measured power ratio be multiplied to convert it to the power ratio that would have been obtained had the same volumes been utilized (neglecting the altitude variation of the cross-section per unit volume).

Utilyzing the power spectrum approximation

$$\overline{|F(s)|^2} = \frac{.221}{s_{1/2}^2} \exp\{-.693(\frac{s}{s_{1/2}})^2\} \qquad (3.6)$$

one can show that

$$\frac{\text{Vol 0 wave}}{\text{Vol X wave}} = 2[1-\exp\{-.693(\frac{\sin 13.2^\circ}{s_{1/2}})\}] \qquad (3.7)$$

where $s_{1/2}$ is the sine of $\theta_{1/2}$ for X wave polarization.

Table 3.3 gives the corrections by which the A_x/A_o ratios associated with the data of Table 3.2 must be multiplied to account for the different scattering volumes for the "X" and the "0" waves. Note that the correction is the reciprocal of the square root of equation (3.7) and that this is strictly a geometrical correction which does not properly account for the differential backscatter cross section as a function of altitude.

Table 3.3 Ratio Corrections As a Function of Altitude

h_{km}	X wave $\theta_{1/2}$	Correction Factor
72	13.2°	1.00
74	17.8	.80
76	20.5	.71

Oblique echoes associated with X waves at altitudes where $\frac{\partial \bar{A}_x}{\partial R}$ is negative can result in substantial errors for the $\bar{A}_x/\bar{A}_o$ ratio resulting in an overestimation of the ratio and an underestimation of the electron density in these regions.

Because shorter pulse lengths have a smaller V_s for a given cone angle, a shortening of the pulse length will not increase the height resolution in those ranges where $\frac{\partial \bar{A}_x}{\partial R} < 0$. A shorter pulse length increases the measured $\bar{A}_x/\bar{A}_o$ ratio at such ranges. A representative plot of $\bar{A}_x/\bar{A}_o$ ratios obtained with 25 and 12.5 μs pulses is shown in Figure 3.2. The ratio is seen to increase for the shorter pulse length where the X-wave amplitude decreases with height. The SNR was large enough not to effect the 12.5 μs measurement.

3.3 Wide Cone Angles and Electron Density Minima. One of the principal goals of this research was to identify causes of erroneous electron density profiles. Two electron density profiles are illustrated in Figure 3.3 and Figure 3.4. The local minima in electron density at 78 km and 80 km are the portions of the profiles in question. Minima which occur below 72 km are not questioned because of possible innacuracies in the ratio measurements caused by interference and noise.

Consider the curve of Figure 3.3. Corresponding X-wave cone angle measurements are shown on the plot. Note the 22.3° cone angle at 78 km where the electron density minimum occurs. A much deeper minimum is shown in Figure 3.4 at 80 km. A cone angle measurement at 80 km was not available for the data of Figure 3.4, but the cone angle had already reached 20.7° at 78 kilometers. The implication of this figure is that local minima in electron density profiles can result from oblique X-wave echoes and altitude smearing. The oblique echoes are frequently associated with regions in which the X-wave amplitudes decrease with increasing altitude.

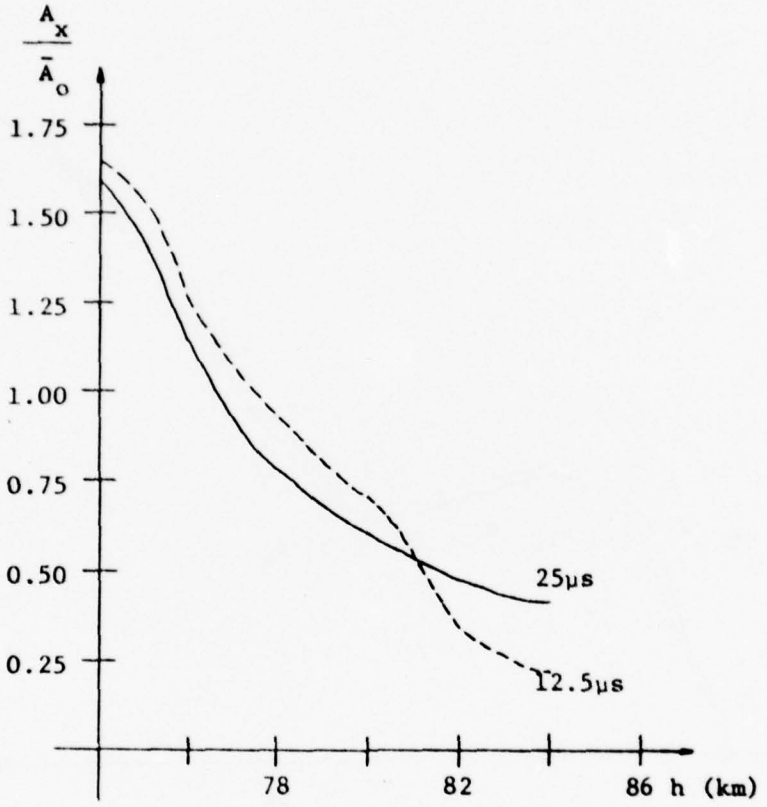

Figure 3.2 Effect of pulse length on measured $\bar{A}_x/\bar{A}_o$ ratios.

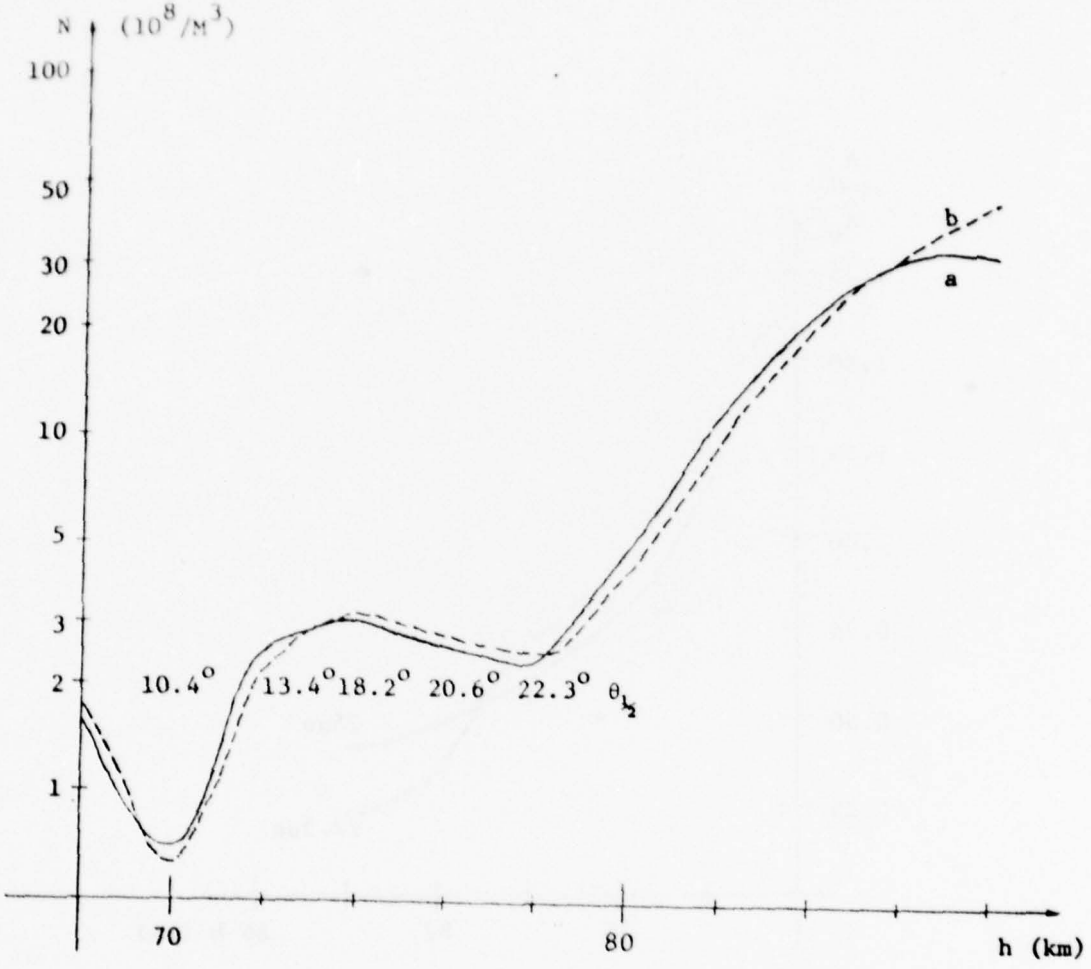

Figure 3.3 Relationship of the X-wave cone angle to the electron density minimum.

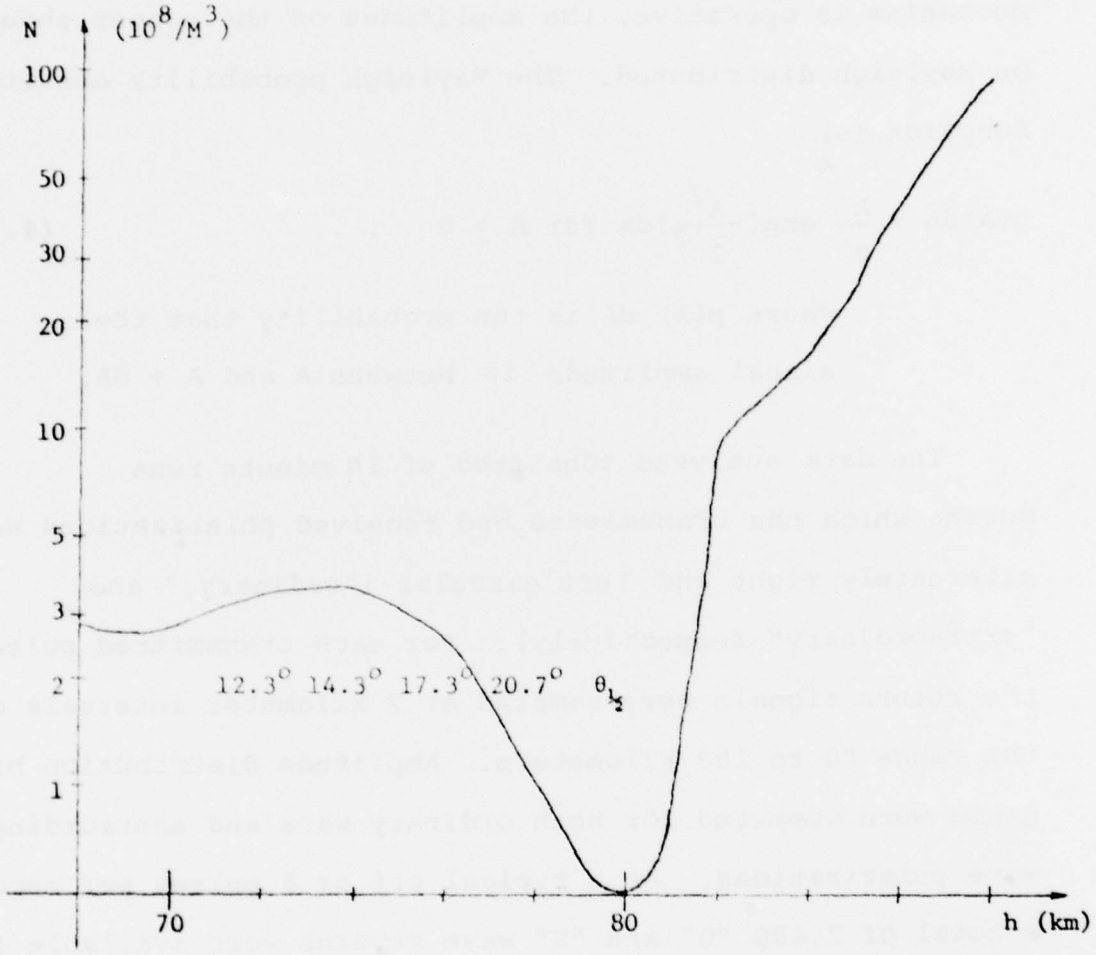

Figure 3.4 Extreme case of an electron density profile minimum.

4. Amplitude Distributions of D Region Echoes

Flood (1968) proposed that D region echoes were caused by scattering from refractive index fluctuations. If this mechanism is operative, the amplitudes of the echoes should be Rayleigh distributed. The Rayleigh probability density function is:

$$p(A)dA = \frac{A}{\sigma^2} \exp\{-\frac{A^2}{2\sigma^2}\}dA \text{ for } A \geq 0 \ . \ . \ . \qquad (4.1)$$

where p(A) dA is the probability that the signal amplitude is between A and A + dA.

The data analyzed consisted of 10 minute runs during which the transmitted and received polarizations were alternately right and left circular ["ordinary," and "extraordinary" respectively]. For each transmitted pulse, the return signals were sampled at 2 kilometer intervals over the range 60 to 100 kilometers. Amplitude distribution histograms were computed for both ordinary wave and extraordinary wave polarizations. At a typical prf of 8 pulses per second, a total of 2,400 "O" and "X" wave returns were available for each 10 minute period. The data were screened for noisy and saturated returns at each altitude. These restrictions effectively set the lowest altitude for which valid data was available at 70 kilometers. Only 1/4 of all the available data runs passed the screening procedure.

The data samples at each altitude were normalized to the sample mean value and eight "bin" histograms were computed.

The Chi-squared hypothesis test using six degrees of freedom (we had normalized the amplitudes) was applied to the histograms. Acceptance or rejection of the Rayleigh hypothesis was set at the 10% level -- i.e., the probability that the differences between the observed (data) distribution of amplitudes and that expected from a true Rayleigh distribution could be caused by sampling error is less than 10%.

A summary of the Chi-squared test results is shown in Table 4.1. The notation in the table is:

ALT = altitude in kilometers

N = number of screened 10 minute observations at that altitude

$\overline{CL\%}$ = mean confidence limit of the N observations

N 10% = number of 10 minute observations that were rejected at the 10% level as not being drawn from a Rayleigh population.

Table 4.1 Summary of Chi-Squared Results

ALT	70	72	74	76	78	80	82	84	86
N	20	23	25	23	26	25	23	24	23
$\overline{CL\%}$	42	39	44	39	41	44	51	41	42
$N_{10\%}$	2	4	2	5	2	2	1	1	2

If the usual five percent confidence cutoff had been used, only 8 data runs would have been rejected (not from a Rayleigh population). The average Chi-squared confidence level of 40% supports the hypothesis that the amplitude distributions are Rayleigh distributed and, by inference, the contention that volume scatter from a continuous distribution of refractive index fluctuations is the source of D region backscatter.

5. Seasonal Variation of D Region Electron Density Profiles

Altitude profiles of the ratio of backscattered amplitude of the extraordinary wave to the backscattered amplitude of the ordinary wave were obtained over an 18 month period. All of these data were collected near local noon (minimum solar zenith angle) when D region electron densities are close to the maximum daily values. These "A_x/A_o" profiles were subjected to a series of screening criteria based upon estimates of signal to interference ratios, number of saturated samples, the number of contigous altitude bins which had "good" signals and the value of the short lag autocorrelation coefficient at each altitude. The data used in this section passed all the screens. In the 18 month period there were 75 data days which were acceptable; these data days were typified by approximately three consecutive (or nearly so) acceptable 10 minute records. If such was the case, the electron density for that day was computed from the average of the three electron density profiles derived from each 10 minute run.

The short lag autocorrelation screen provides a way to quantify signal to interference ratios. It was observed that D region normalized autocorrelation functions maintained substantially high values (greater than 0.7) for lags as long as 1/4 second while interference tended to decorrelate to values of .2 to .4 in 1/8th second. Consequently, we required the echoes to have a normalized correlation function of at least 0.75 at a lag of 1/4th second.

Electron density profiles calculated from an average of three consecutive 10 minute Ax/Ao profiles were compared with electron density profiles computed by averaging three consecutive electron density profiles computed for each 10 minute period. While there were differences between the daily average values so computed, they were minimal and in our opinion of no consequence. Consequently in the data reported herein, the daily average electron density profile was computed from the average of the electron density profiles derived from 10 minute runs taken on that day.

The 75 average day profiles were divided into Spring, Summer, Fall, and Winter, and all density profiles within that category averaged to produce an average electron density profile for each season. The average electron density profiles for summer and winter and the equinoctial periods are plotted in Figure 5.1. The measurements show a definite difference between summer and winter electron densities at altitudes above 78 kilometers -- the one sigma error bars are well separated. Below 78 kilomters there is nothing to distinguish the two profiles. The equinoctial profiles above 78 kilometers lie between the

winter and summer curves although below 78 kilometers it appears that electron densities are greater for the equinoctial months. Table 5.1 lists, as a function of altitude, the seasonal mean values and the associated σ value.

The behavior of the seasonal variation above 78 kilometers is consistent with primarily solar photon control and the behavior below 78 kilometers points to the influence of energetic particles at these altitudes.

The use of average profiles can be misleading in characterizing the D region electron density profiles. Figure 5.2 shows the average winter profile with the associated 1σ error bars at each altitude. Also plotted are electron density values for five selected winter days with anomalously high electron densities. The electron density values for each of these five days are the average of at least 3 consecutive 10 minute curves and exceed the average plus one σ winter values. Table 5.2 lists, as a function of altitude, the electron density values for each of these 5 days along with the mean and the $M \pm \sigma$ for an average winter day.

The absorption on these "amomalous" days was high, but there are at least two different kinds of anomalous days. The electron densities deduced for 1/8/77, 1/9/77, and 2/12/78 are approximately twice the average winter values in the region between 80 and 90 kilometers and are equal to, or lower than the average mean winter day at altitudes below 80 kilometers. On the other hand, the data of 12/31/77 and 1/1/78 indicate higher than normal values

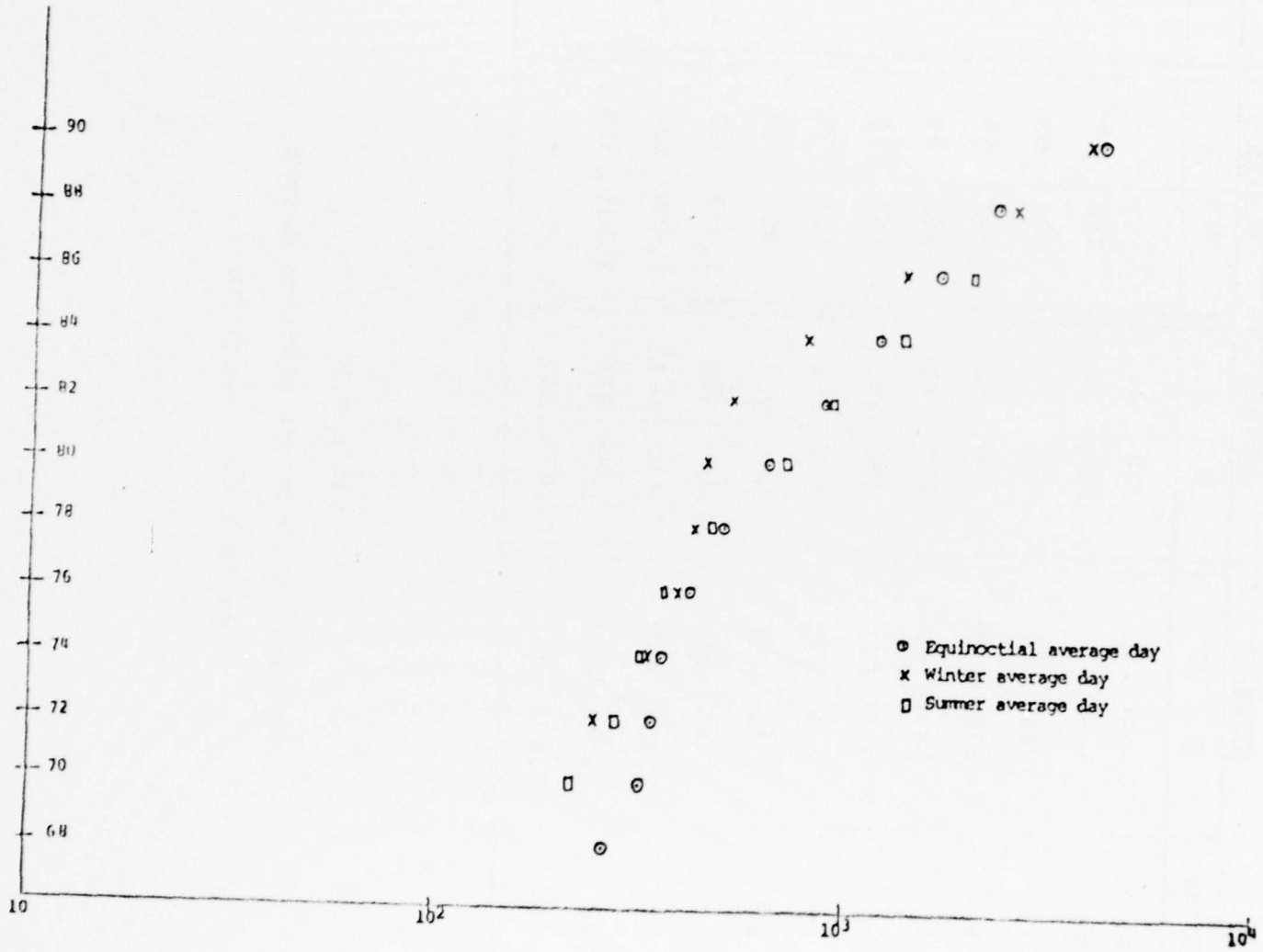

Figure 5.1 Comparison of average profiles for equinoctial, summer and winter days

	WINTER		SPRING		SUMMER		FALL	
ALTITUDE	M	σ	M	σ	M	σ	M	σ
68	---	---	260	44	---	---	---	---
70	---	---	319	50	216	57	283	34
72	244	57	337	65	274	63	328	61
74	328	115	354	82	313	56	330	50
76	388	140	413	87	356	99	384	47
78	425	153	495	102	461	179	475	103
80	447	151	636	161	688	274	620	183
82	519	188	880	227	896	233	851	243
84	786	270	1,180	260	1,353	302	1,223	290
86	1,388	498	1,669	514	1,998	536	1,601	383
88	2,561	1,063	2,280	950	2,135	339	---	---
90	3,802	911	4,072	127	---	---	---	---

Table 5.1

Seasonal Averages of Electron Density

(per CM^3) at Raleigh, N. C.

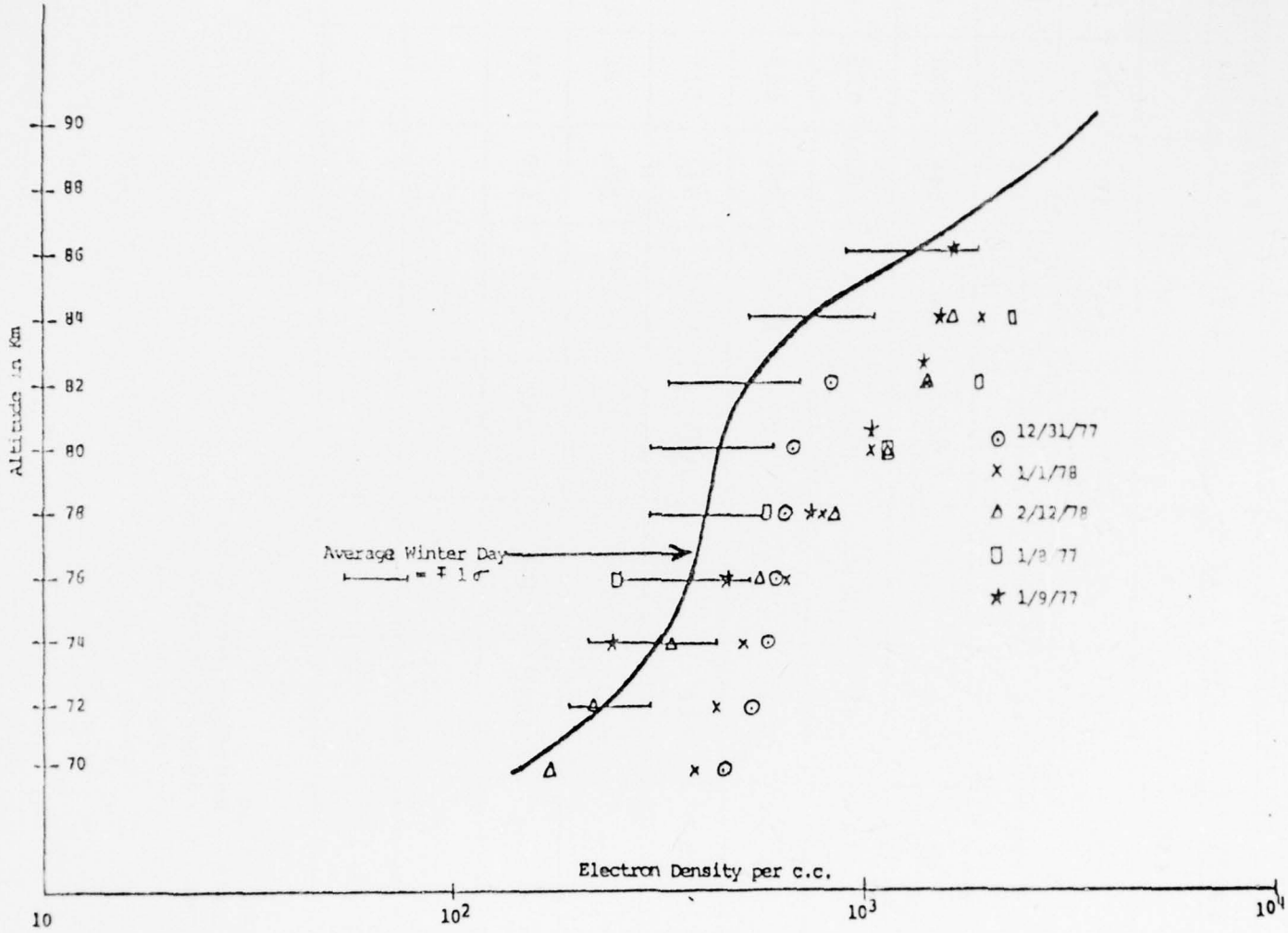

Figure 5.2 Anomalous winter days

5.2

Table 5.2 Electron Density (Electrons/cc) on Anomalous Winter Days

Alt. in KM.	Electron Density in Electrons/Cubic Centimeter							
						Average Winter Day		
	12/31/77	1/1/78	2/12/78	1/8/77	1/9/77	M-σ	M	M+σ
70	456	382	171	--	--			
72	529	435	213	--	--	187	244	301
74	580	506	337	282	239	208	323	438
76	615	616	550	241	467	248	388	528
78	643	790	834	576	743	302	425	548
80	670	1052	1151	1125	1052	296	447	598
82	822	1428	1441	1907	1385	331	519	707
84	--	1940	1621	2280	1537	516	786	1056
86	--	2572?	2098	3428?	1634	890	1388	1886
88	--	--	2643?	--	--			
90								

M = mean value
M-σ = mean - standard deviation
M+σ = mean + standard deviation

below 80 kilometers and just possibly twice the average values up to 84 kilometers where good data cease. If these five days are examples of days of anomalously high winter absorption, it is clear that the major absorption occurs above 90 kilometers and that the values reported here for the 80-90 kilometer region (roughly twice the average winter value) are less than electron density enhancements which have been reported in the literature (factors of 2-4).

Discussion

The equipment used in these experiments included a 100 kilowatt peak pulse power transmitter operating at a frequency of 2.66 MHz with adjustable pulse lengths (25 microseconds for all experiments in this report) and with pulse repetition frequency selectable from 2, 4, 8, 16, and 32 pulses per second. Four crossed dipole antennas were used as the main transmitting array and were used as the receiving array for electron density profiling (part 5 of this report) and D region amplitude distribution (part 4). Transmitted and received polarizations were selectable on a pulse to pulse basis, controlled by a digital logic unit (DLU).

The DLU in addition to controlling transmitter and receiver antennas also controls the gain of the receiver, making possible a gain change within the 13.3 microseconds between successive altitude samples at 2 kilometer intervals. The receiver output is sampled at 2 km intervals and converted to an eight bit digital word which is buffered by the DLU and recorded on a nine track

digital tape recorder. The receiver utilized a gain programmable intermediate frequency amplifier and a "super" linear detector -- linear to within one count of an eight bit (256 count) A/D converter at any fixed receiver gain setting.

The Raleigh field site is by no means an optimum site for a D region experiment. It is within 150 miles of a very active sea cast and the marine band (2.66 MHz is in the middle of the marine band) is in constant commercial use. We have found that minimum interference levels are obtained on weekends -- on Saturdays and Sundays. Nonetheless, attempts to collect interference free data were made throughout the week. The fact that we collected a large quantity of "valid" data at on site was solely due to the persistence of the junior authors of this report.

Descriptions of the electronic circuits utilized can be found in the master's theses of Glace (1976), Green (1977), Harris (1977), Dix (1976), Caverly (1978), Collins (1978), and Shirley (1978). Additional equipment and analytical descriptions can be found in the Ph.D. thesis by Turner (1977).

Summary

We have shown partial verification of the RPASA. Except on rare occasions, interference precluded accurate measurement of the phase of the complex correlation functions although on the few occasions when interference was low, the phase was consistent with a valid RPASA.

Cone angle of arrival measurements have shown that, for the Raleigh site, altitude smearing may be a problem between 74 and 80 kilometers for the partial reflection experiment. While these problems have been identified, alleviation of the effects of

oblique echoes has not been sought in the data reduction procedures outlined in section 5 of this study. Consequently some of the profiles which make up the seasonal averages shown in this report may have suffered from altitude smearing and (over the 74-80 kilometer range) concommittant electron density minima

We have identified three potential causes for erroneous electron density minima. They are:

1. Overspecifying the order of the polynomial for electron density as a function of altitude which is used to fit, in a least squared error sense, the Ax/Ao data points.
2. Using a less accurate model for the refractive index in the D region. This potential cause is minimized by using short transmitted pulse lenghts.
3. Different scattering volumes for the X and 0 waves (due to wide cone angles and altitude smearing) cause apparent electron density minima.

We have attempted to minimize the effect of all three causes by using a polynomial whose order was less than one half the number of data points, using the Flood (1979) approximation to the Sen-Wyller theory of refractive index and by using a 25 microsecond pulse length. There is no way to minimize the physical reality of increased cone angles for X waves when they occur.

The electron densities were deduced from the formulation proposed by Belrose and Burke (1964) using the Flood's (1979)

approximation to the refractive index. The fact that the average seasonal electron density profiles do not show local minima is undoubtedly the result of averaging a large number of profiles, some of which show apparent minima at various altitudes. The averaging process will tend to suppress even true local minima if there is no consistent altitude at which the minima occur.

A word of caution is required in the use of the seasonally averaged profiles. There is an apparent large day to day variation of electron density profiles as seen at Raleigh. An average profile is precisely what it says it is -- an average and deviation from the average should be expected for any particular profile.

The amplitude distribution of D region echoes has been shown to be consistent with a Rayleigh distribution -- thereby lending support to the proposition that D region backscatter is due to volume scattering from refractive index fluctuation.

Acknowledgements

This report is based on the following theses submitted to N. C. State University.

Turner, Harvey N. Jr., "Some Inherent Limitations to the Accuracy of D Region Electron Density Profiles Obtained by the Differential Absorption Partial Reflection Technique," Ph.D. Thesis, 1977.

Collins, Samuel David Jr., "Cone Angle Measurements of the E Region and Amplitude Distributions for the D Region," an MS Thesis, 1978.

Shirley, Thomas Franklin, Jr., "D Region Electron Density Profiles for Raleigh, North Carolina," an MS Thesis, 1978.

The equipment used in this research is described in the following MS theses submitted to N. C. State University:

Green, J. Hugh, Jr., "A 2.66 MHz Pulsed Exciter," 1976.

Glace, Dean Alexander, "Design, Construction, and Testing of a 100 Kilowatt Peak Pulse Power Transmitter Used at H. F. Frequencies," 1974.

Dix, James F., "A Data Acquisition and Control System for Ionospheric Research," 1975.

Harris, Mark A., "A Receiving System for Ionospheric Research," 1975.

List of References

Belrose, J. S., and M. J. Burke, 1964, "A Study of the Lower Ionosphere Using Partial Reflections," Journal Geophysical Research, Vol. 69, p. 2799.

Flood, W. A., 1968, "Revised Theory for Partial Reflection D Region Measurements," Journal of Geophysical Research, Vol. 73, p. 5585.

Flood, W. A., 1979, "A D Region Mid-and-High-Latitude Approximation to the Sen-Wyller Refractive Index Equations," [unpublished 1976], to be submitted to Radio Science.

Von Biel, H. A., 1970, Unpublished Doctoral Thesis presented to University of Canterburg, Christchurch, New Zealand.